Energy and Built Environment 5 (2024) 130–142

Contents lists available at ScienceDirect

Energy and Built Environment

journal homepage: http://www.keaipublishing.com/en/journals/energy-and-built-environment/

On the optimisation of age of the air in the breathing zone of floor heating systems: The role of ventilation design

Aminhossein Jahanbin[a,b,*], Giovanni Semprini[a]

[a] Department of Industrial Engineering (DIN), Alma Mater Studiorum - University of Bologna, Viale Risorgimento 2, 40136 Bologna, Italy
[b] CIRI - Centro Interdipartimentale di Ricerca Industriale Edilizia e Costruzioni, Alma Mater Studiorum - University of Bologna, Via del Lazzaretto 15/5, 40131 Bologna, Italy

ARTICLE INFO

Keywords:
Age of the air
Indoor air quality
Ventilation
Floor heating
CFD

ABSTRACT

For a mechanically ventilated space, the nominal age of the air can be obtained by the reciprocal of the air change rate. However, values of the local mean age of the air in practice may differ to some extent from the nominal one since the nominal time constant employs as reference the theoretical optimum model. This discrepancy could become more prominent in spaces conditioning with both ventilation and heating system where the indoor air pattern is affected by turbulent mixed convection flow. Given importance of knowledge on the distribution of age of the air in these spaces, the present study provides insights on how ventilation design in floor heating systems can optimise the delivery of fresh air into the breathing zone. In this context, by establishing a computational fluid dynamic (CFD) model validated against experimental data, the local mean age of the air as well as the indoor air quality (IAQ) indices in the breathing zone of the floor heating system are examined under different ventilation modes. Six different ventilation scenarios are regarded in order to find the optimal ventilation design in terms of the delivery of the fresh air and ventilation effectiveness in occupied space. Furthermore, the integrated effects of the floor temperature and inlet supply temperature along with the ventilation design on the distribution of local age of the air are addressed. The obtained results indicate that the up-supply ventilation strategy is more efficient than down-supply one in the ventilation effectiveness and delivery of fresh air into the breathing zone. Moreover, it is shown that the mean age of the air in the breathing zone of the up-supply ventilation increases with increment of the *Ri* (Richardson number), whereas an increase in *Ri* improves the delivery of fresh air in down-supply mode. For a given floor temperature, the similar trend is also observed in the variation of age of the air with the characteristic temperature of supply inlet, namely the temperature difference between inlet supply and surrounding walls.

1. Introduction

Over the past decade, the indoor air quality (IAQ) has been a global concern of the public, governments, and scientific community since it is well-known that IAQ is a critical issue related to human health, satisfaction and productivity [1,2]. The importance of healthy indoor air has recently been exacerbated by the spread of COVID-19 due to the fact that careful air quality control can prevent airborne virus transmission in occupied spaces [3]. The air quality within an occupied space depends on several parameters such as the indoor contaminants, nature of air movement and HVAC (heating, ventilation, and air conditioning) system. In this context, building ventilation plays a key role by handling the quantity of air required in the indoor space under specific environmental conditions. Many studies have addressed the relationship between inadequate ventilation rate in built environments and human health-related problems [4–6].

Although the main purpose of applying different types of the ventilation system is to remove heat and contaminants from the occupied space, the delivery of fresh air and contaminant distribution are the direct function of indoor air movement which could significantly affect the IAQ within a ventilated space [7]. Indeed, each specific type of the ventilation system would have its unique impact on IAQ since the indoor air movement is dramatically dependant upon the ventilation design as well as the geometrical and physical parameters of the enclosure [8–10]. Hence, an optimal design of ventilation system could contribute to an improved IAQ while reducing the minimum volumetric flow rate which leads to a remarkable energy saving.

The quality of indoor air can be measured by the absolute value of contaminant concentration, ventilation effectiveness and relative indicators such as the age of the air [11]. The latter, namely the local mean

* Corresponding author.
E-mail address: aminhossein.jahanbin@unibo.it (A. Jahanbin).

https://doi.org/10.1016/j.enbenv.2022.08.005
Received 23 July 2022; Received in revised form 22 August 2022; Accepted 27 August 2022
Available online 29 August 2022
2666-1233/Copyright © 2022 Southwest Jiatong University. Publishing services by Elsevier B.V. on behalf of KeAi Communication Co. Ltd. This is an open access article under the CC BY-NC-ND license (http://creativecommons.org/licenses/by-nc-nd/4.0/)

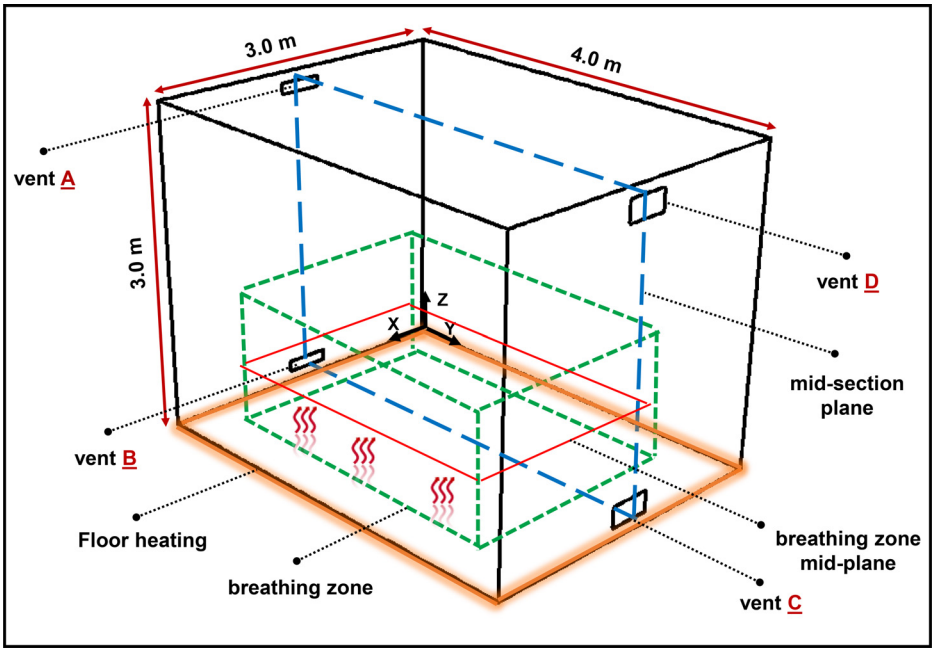

Fig. 1. Schematic and details of the case under study.

age of air, is a statistical value addressing the time that all molecules of fresh air require to move from supply inlet to an arbitrary point [12]. The age of the air is an important index identifying the quality of indoor air; the younger the age of the air, the better the indoor air quality. Using this value, it is possible to determine the air change efficiency of the room, recommended for dwellings where no local source of contamination can be located and, at the same time, as a guarantee of desired air quality throughout the entire volume of the room [13] .

The local mean age of the air can be calculated by either experiments, i.e. the tracer gas decay method [14], or computational fluid dynamic (CFD) simulations. The literature review shows that there are several research articles that have employed the concept of the age of the air for evaluation of IAQ in ventilated spaces. For instance, a numerical analysis was performed by Ning et al. [15] on the age of the air in breathing zone of a bedroom with different heights of conditioned air supply inlet. They found that placing the supply inlet at a lower level is more effective in both removing contaminants and saving energy. The local mean age of air in a naturally ventilated office was evaluated by Buratti et al. [16] through both tracer gas measurements and numerical simulations. By comparing experimental and numerical results, it was concluded that numerical model could be very useful for the prediction of the mean age of air, allowing both costs and time saving in the evaluation of IAQ.

Through numerical evaluation of the mean age of the air, air quality in a naturally cross-ventilated educational building was investigated by Diaz-Calderon et al. [17]. The obtained results showed that the current natural ventilation standards, considering values of the air change per hour, may lead to wrong decision in providing a healthy indoor air. Ahn et al. [18] investigated ventilation and energy performance of partitioned office spaces under mixing and displacement ventilation. Their numerical results indicated that local age of the air significantly varies with both diffuser arrangement and ventilation strategy in addition to that the displacement ventilation requires shorter time for the partitioned room to achieve an indoor set-point temperature, compared to the mixing ventilation.

For a mechanically ventilated space, a commonly used criterion for the local mean age of air is the nominal time constant or nominal age of the air. The nominal time constant of a ventilated space is the ratio of the air volume to the air flow rate, i.e., the reciprocal of the air change rate, and for flows without short-circuiting, it is equal to the local mean age at air exit [19]. However, the value of local mean age of the air in practice may differ to some extent from the nominal one since the nominal constant employs as reference the theoretical optimum model or “ideal piston flow model”. This issue could be critical in spaces that employ the lowest allowable air change rate to minimise the ventilation energy consumption.

Indeed, the local mean age of the air can be considered as a function of the architectural parameters, the ventilation system design; the location of supply inlet and exhaust vents as well as the supply inlet variables, and the indoor air pattern [20,21] . The role of the latter in delivery of the fresh air becomes more prominent when the indoor airflow is affected by both the ventilation system and heat source, i.e., the complex relation between turbulent airflow and temperature driven by mixed convection. Therefore, accurate understanding of the distribution of local age of the air in each HVAC system is of significant importance as it is related to determining the required ventilation rate in occupied spaces.

Based on the literature review above, it is noticed that the available studies have mainly neglected integrated effects of the ventilation design and heat source on distribution of local mean age of the air. Given the importance of knowledge on distribution of age of the air in combined ventilation and heating systems, the present study aims to investigate the delivery of fresh air in the breathing zone of a typical ventilated space equipped with the floor heating system. In this context, six different ventilation scenarios are introduced and the distribution of the age of the air and the ventilation effectiveness in each case are compared under different ventilation rates in order to find the optimal ventilation design. Furthermore, the integrated effects of the floor temperature and inlet supply temperature along with the ventilation design on the local age of the air are addressed. Finally, the obtained results are verified by monitoring the CO_2 decay rate in the breathing zone of various cases. Findings of the present study are expected to provide insights on optimal ventilation design in floor heating systems.

2. Methods

2.1. Cases description

The domain under examination is a typical room with dimensions of 4.0 m (length) × 3.0 m (width) × 3.0 m (height) and a volume of 36.0 m^3. The enclosure is equipped with the floor heating system as well

Table 1
Details of different scenarios considered for the ventilation mode.

scenario	supply mode	exhaust mode	inlet vent	outlet vent
S-1	up-supply	down-exhaust	A	C
S-2	up-supply	up-exhaust	A	D
S-3	down-supply	up-exhaust	B	D
S-4	down-supply	down-exhaust	B	C
S-5	up-supply	down-exhaust	A	B
S-6	down-supply	up-exhaust	B	A

as ventilation vents (supply inlet and outlet) located on the symmetrical position of side walls with 10 cm distance from the ceiling and the floor. The inlet vent with dimensions of 0.4 m (length)× 0.1 m (width) and the outlet with a size twice as large as the inlet (0.08 m^2) were considered. The dimension of inlet and outlet vents were selected according to the recommend aspect ratio of inlet and outlet vents by Chen et al. [22] to achieve better ventilation efficiency. Fig. 1 illustrates the schematic and features of the room under examination.

In order to evaluate the air quality in the breathing zone, the definition of "breathing zone" from the ANSI/ASHRAE standard 62.1 [23] was regarded, namely "the region within an occupied space between planes 3 and 72 in (75 and 1800 mm) above the floor and more than 2 ft (600 mm) from the walls or fixed air-conditioning equipment". The breathing zone as well as its horizontal mid-plane have been marked in Fig. 1.

In terms of the ventilation design, six different scenarios were considered in the present study to find out the most effective one in the floor heating system. In this context, three up-supply and three down-supply cases were selected, namely all possible symmetrical ventilation modes. Details of various scenarios and their corresponding inlet and outlet vents are reported in Table 1.

To investigate the combined effects of ventilation strategy and ventilation rate on distribution of the local age of the air, three values of the inlet air velocity corresponding to rather low values of the air change per hour (ACH) were considered, which fall within the scope of this study. Indeed, the difference between the nominal and local age of the air in spaces ventilating with low ACHs may be a critical issue, as stated in the Introduction section. Hence, in the present study, low values of the ACH have been considered in order to highlight better this difference. Regarded values of the ACH are 0.2, 0.4 and 0.6, associated with values of the nominal age of the air equal to 6000, 9000 and 18000s, respectively. Table 2 reports the characteristics of different ventilation rates considered in the present study.

In addition, four inlet air temperatures, namely 16, 18, 20 and 22 °C, and four floor temperatures, namely 23, 25, 27 and 29 °C, were considered in order to address the role of supply air temperature and floor heating system (mixed convection) in distribution of fresh air in the breathing zone. For the baseline simulations, namely various scenarios for ventilation (Section 4.1), the inlet air temperature and floor temperature were regarded equal to 20 and 25 °C, respectively, as adopted in a similar study [24]. According to the ASHRAE Standard 55 [25], recommended range of floor temperatures design for those wearing normal footwear is above 66°F (19°C) in cooling condition and below 84°F (29°C) in heating condition. In this context, the range 74°F - 77°F (23°C - 25°C) is a condition where the least amount of people will complain (6%) or the most amount of people will be satisfied (94%).

It is noteworthy to mention that, for different simulations cases, the operating conditions were regarded as to satisfy the thermal comfort condition in the occupied space. The mean air temperature and velocity in the occupied zone are in the range 20.76 °C – 22.27 °C and 0.051 m/s – 0.085 m/s. Moreover, the maximum floor temperature is 29 °C and drought rate does not exceed 4.7%.

A total of thirty-seven numerical simulations under different operating conditions were carried out. Firstly, the merit and drawback of each ventilation scenario (Table 1) in terms of the IAQ are evaluated under different ventilation rates. Then, combined impacts of the supply air temperature and floor heating system along with the ventilation design on the local mean age of the air in breathing zone were investigated. The process of the whole analysis conducted in this study is demonstrated in Fig. 2.

2.2. Numerical setup

The indoor airflow is a turbulent flow driven by buoyancy force and momentum. The airflow was supposed to be incompressible due to the small gradient of the pressure and low air velocity. It was assumed that thermophysical properties of the air are constant except the density, which was estimated through the Boussinesq approximation as a linear function of the air temperature; $\rho = \rho_0[1 - \beta(T - T_0)]$. The indoor air was assumed as the humid air and the corresponding thermal properties were estimated at relative humidity of 50% and reference temperature of 20 °C.

For modelling the indoor turbulent airflow, the Reynolds Average Navier-Stokes (RANS) method was considered and, in analogy with similar studies [26,27], the RNG (Renormalisation Group) k-ε model was selected for the numerical simulation. The enhanced wall treatment method was employed to model near-wall turbulent flow. This method is based on the turbulent Reynolds number, $Re_y = \rho y \kappa^{0.5} \mu^{-1}$, combining a viscosity-affected layer and fully turbulent region with enhanced wall functions [28]. The radiation heat transfer inside the computational domain was modelled by employing the discrete ordinates (DO) radiation model, which solves the radiative transfer equation for a finite number of discrete solid angles.

The polyhedral grid strategy was used to mesh the computational domain. The domain was preliminary meshed with unstructured tetrahedral elements, which then converted to polyhedral mesh in order to optimise the grid quality. A non-uniform mesh strategy was regarded, with a more dense mesh in vicinity of solid walls and ventilation vents, and a smoother mesh density with expansion rate for far-field regions. To justify adoption of the enhanced wall function in RNG turbulence model, it was ensured that, for a given Reynolds number, the distance from the wall remains below $y^+ = 5$.

The 3D governing equations in this study were solved by means of the finite volume method (FVM), implemented through ANSYS Fluent software. A pressure-based solver was chosen as a solution method and the second-order upwind scheme was adopted in order to convert the governing equations into a set of algebraic discretized equations. For coupling of the velocity and pressure terms, the SIMPLE (Semi-Implicit Method for Pressure-Linked Equation) algorithm was employed.

The convergence of solutions was monitored by controlling the history of residuals. In order to optimise the solution convergence, under-relaxation factors for momentum and turbulence terms were utilised. The convergence criteria for the momentum terms, energy equations

Table 2
Characteristics of different ventilation rates regarded in the present study.

	volume flow rate (m^3/h)	inlet velocity (m/s)	air change per hour (ACH)	nominal age of the air (s)
1	7.2	0.050	0.2	6000
2	14.4	0.100	0.4	9000
3	21.6	0.150	0.6	18,000

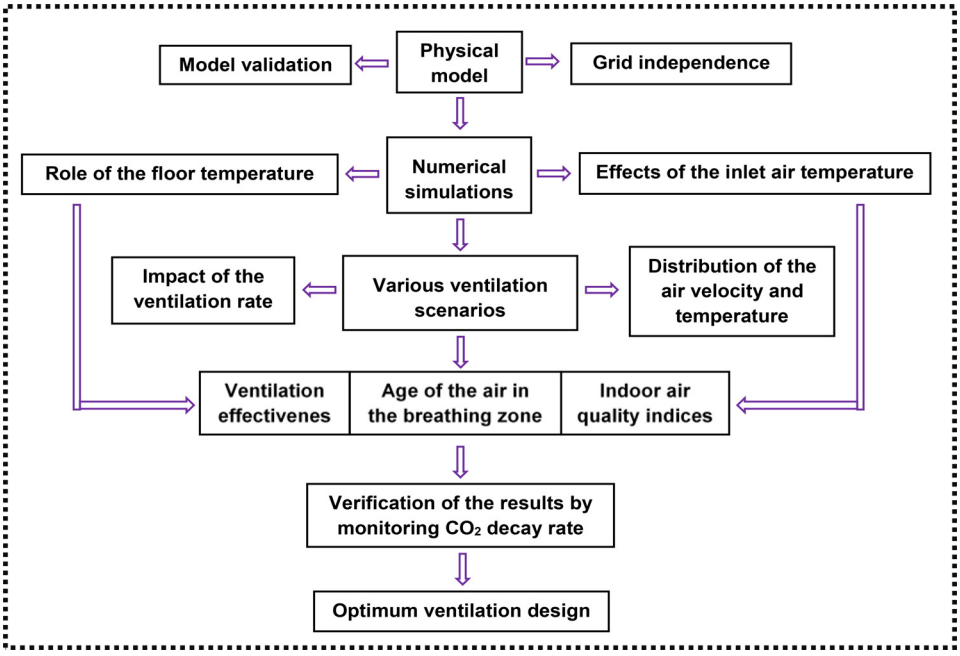

Fig. 2. A block diagram to describe the structure of the present study.

and USD (user-defined scalar) was assumed as 10^{-4}, 10^{-6} and 10^{-7}, respectively. As a final check of the solution accuracy, the heat flux balance across the domain boundaries was monitored to meet the discrepancy criteria of < 0.1%.

2.3. Governing equations

The governing equations of the mass, momentum and energy balance for the steady-state turbulent flow are given by:

$$\nabla \cdot (\rho \vec{v}) = 0 \tag{1}$$

$$\rho_0(\vec{v} \cdot \nabla)\vec{v} = -\nabla(p + \rho_0 g z) + \rho_0 g \beta (T - T_0)\nabla z + \nabla \cdot \tilde{\tau}_{eff} \tag{2}$$

$$\nabla \cdot \left(\vec{v}(\rho e + p)\right) = \nabla \cdot \left[(k + k_t)\nabla T + \tilde{\tau}_{eff} \cdot \vec{v}\right] \tag{3}$$

where in Eqs. (1 – 3),$\vec{v}$ is the velocity vector, p is the pressure, β is the air thermal expansion coefficient and e is the energy per unit mass;$e = h - p/\rho + v^2/2$ and h is the specific enthalpy. Furthermore, $\tilde{\tau}_{eff}$ is the effective stress tensor which is given by$\tilde{\tau}_{eff} = \tilde{\tau} + \tilde{\tau}_t$, and in the Boussinesq approximation can be expressed as:

$$\tilde{\tau} = \mu\left(\nabla \vec{v} + \nabla \vec{v}^T\right); \quad \tilde{\tau}_t = \mu_t\left(\nabla \vec{v} + \nabla \vec{v}^T\right) \tag{4}$$

The turbulence RNG κ-ε model's governing equations are given by [29]:

$$\nabla \cdot \left(\rho \kappa \vec{v}\right) = \nabla \cdot \left(\alpha_\kappa \mu_{eff} \nabla_\kappa\right) + 2\mu_t E_{ij} E_{ij} - \rho\varepsilon \tag{5}$$

$$\nabla \cdot \left(\rho \varepsilon \vec{v}\right) = \nabla \cdot \left(\alpha_\varepsilon \mu_{eff} \nabla \varepsilon\right) + C^*_{1\varepsilon} \frac{\varepsilon}{\kappa} 2\mu_t E_{ij} E_{ij} - C_{2\varepsilon} \rho \frac{\varepsilon^2}{\kappa} \tag{6}$$

where E_{ij} is the strain rate and $C^*_{1\varepsilon}$ and $C_{2\varepsilon}$ are the RNG turbulence coefficients that have been adopted identical to those employed in Ref. [30]. In Eqs. (4- 6), μ_{eff} and μ_t are defined as:

$$\mu_{eff} = \mu + \mu_t; \mu_t = \rho C_\mu \frac{\kappa^2}{\varepsilon} \tag{7}$$

A transport model has been used in numerical model to analyse the age of the air. Indeed, the local mean age of the air is a passive quantity that is determined in steady-state condition by the solution of airflow equations. To obtain the local mean age of the air, a user-defined scalar (UDS) was incorporated into the CFD model; one additional convection-diffusion equation was solved to calculate the transport of an arbitrary scalarφ_i, which can be expressed in the following form:

$$\nabla.\left(\rho \vec{v} \varphi_i - \xi_i \nabla \varphi_i\right) = S_{\varphi_i} \tag{8}$$

where ξ_i and S_{φ_i} are the diffusion coefficient and source term of the scalarφ_i. The diffusion term ξ_i was compiled in numerical code via a user-defined function (UDF) to account for turbulent diffusion. It can be obtained from the effective viscosity of the air (μ_{eff}) [31]:

$$\xi_i = \left(2.88 \times 10^{-5}\right)\rho + \frac{\mu_{eff}}{Sc_t} \tag{9}$$

where$Sc_t$is the turbulent Schmidt number.

In order to evaluate the mean age of the air in the breathing zone, two normalised parameters are introduced, i.e. τ^* and Ω, defined as:

$$\tau^* = \frac{\bar{\tau}_{bz}}{\tau_n} \tag{10}$$

$$\Omega = \frac{\tau_n - \bar{\tau}_{bz}}{\tau_r} \tag{11}$$

where $\bar{\tau}_{bz}$is the mean age of the air in the breathing zone (s), $\tau_n$is the nominal age of the air in the room (s) that can be calculated as the ratio of the volume of the room (m^3) to volumetric fresh airflow (m^3/s), and $\tau_r$is the air renovation time (s) which is expressed by:

$$\tau_r = 2\bar{\tau}_m \tag{12}$$

where $\bar{\tau}_m$is the spatial average of mean age of the air in the room. In fact, Eq. (11) is beneficial in quantitative assessment of age of the air in the breathing zone for different ventilation strategies; larger values of numerator (positive) and lower values of denominator indicate a better delivery of fresh air into the breathing zone.

The ventilation effectiveness in the breathing zone (E_{bz}) can be evaluated as the ratio of the age of the air at ventilation outlet to the mean age of the air in the breathing zone [15]:

$$E_{bz} = \frac{\tau_{out}}{\bar{\tau}_{bz}} \tag{13}$$

The room air change efficiency (*RACE*) is calculated as the ratio of age of the air at outlet to the air renovation time in the room [32]:

$$RACE = \frac{\tau_{out}}{\bar{\tau}_r} \times 100 \tag{14}$$

Table 3
Summary of the adopted boundary conditions.

boundary	conditions (momentum, thermal, radiation and UDS)
supply inlet	velocity inlet, v_{in} =0.05, 0.10 and 0.15 m/s (Table 2), T_{in} = 16, 18, 20 and 22 °C, turbulence intensity=4% and length scale = 0.01 m, φ_i =0
outlet	pressure outlet, $\partial\varphi_i / \partial x_i$ =0
floor	no-slip, isothermal; T = 23, 25, 27 and 29 °C, ε=0.9, $\partial\varphi_i / \partial x_i$ =0
ceiling	no-slip, adiabatic, ε=0.9, $\partial\varphi_i / \partial x_i$ =0
side walls	no-slip, isothermal; T = 20 °C, ε=0.9, $\partial\varphi_i / \partial x_i$ =0

Table 4
Mesh independence of the results: comparison of the mean air temperature, velocity magnitude and normalised age of the air.

mesh no.	elements		T	v	τ^*
	tetrahedral	polyhedral	(°C)	(m/s)	–
1	2173,439	388,212	21.346	0.069	0.983
2	2703,287	477,367	21.337	0.065	0.987
3	3670,439	637,109	21.322	0.063	0.985
4	4314,522	774,677	21.327	0.066	0.988
5	4782,660	814,432	21.339	0.064	0.986

To provide a better comparison for age of the air in the breathing zone under different operating temperatures of both floor and supplied air, two characteristic temperature differences are introduced as follows:

$$\theta_f = T_f - T_w \tag{15}$$

$$\theta_{in} = T_{in} - T_w \tag{16}$$

where T_f, T_w and T_{in} stand for the temperature of floor surface, surrounding walls and inlet supply air, respectively.

2.4. Boundary conditions

As the boundary condition, at the air supply inlets, the velocity inlet condition with specified velocity and temperature was considered and the pressure outlet condition was applied at outlets. For the turbulence boundary condition, turbulent viscosity was calculated based on the turbulent intensity and turbulent length scale. A non-slip condition was imposed on all solid walls. All solid surfaces were considered to be opaque with corresponding values of internal emissivity (ε). According to similar studies [24,33], the ceiling surface was considered as adiabatic while side walls were regarded as isothermal. The floor surface was also considered as isothermal at various temperature levels. Moreover, the infiltration effect was ignored since the ventilation room usually has a positive pressure. Regarding the transport model for age of the air in Eq. (8), the boundary conditions are a zero gradient at air outlet and at solid wall surfaces, and a zero value at air supply inlet. The summary of adopted boundary conditions is reported in Table 3.

3. Model validation

3.1. Grid independence of the results

The mesh independence of the results was checked by comparing mean values of the air temperature, velocity and normalised age of the air obtained by five different grids. As an operating condition, the *S*-1 case with an intermediate inlet velocity, namely ACH=0.4, was considered. Table 4 reports the number of tetrahedral and polyhedral elements in each mesh as well as their corresponding mean values of the air temperature, velocity magnitude and normalised age of the air. The table shows that discrepancies between values of these parameters obtained by different meshes are marginal. Regarding both accuracy and computational efficiency, mesh 2 was selected for final computations. The maximum absolute discrepancy of mean values of the air temperature, velocity and normalised age of the air from the selected mesh is equal to 0.07, 2.12, and 0.18%, respectively, implying the mesh independence of the results.

3.2. Validation of numerical model

In order to validate the numerical model, the results obtained by numerical simulations are compared with experimental data of Chen et al. [22]. The experiments were performed in a test chamber with dimensions of 1.0 m (x) × 1.0 m (y) × 1.0 m (z) with an identical inlet and outlet vent size equal to 0.18×0.05 m^2. The air enters into the room from the up-supply vent and is discharged from the outlet vent, similar to the scenario *S*-1 in Table 1. Measurements were carried out at room temperature (20 °C) by an anemometer with range of 0–5 m/s and error of 0.01 m/s. The velocity magnitude in x-direction was measured along mid-line of the test chamber at seven points for three different values of inlet velocity, namely 0.111, 0.287 and 0.444 m/s. The characteristics of employed numerical model for model validation is identical to that described in Section 2.2.

Fig. 3 compares the simulated and measured normalised x-velocity magnitude along the mid-line of the chamber. The x-velocity magnitude and position along z direction are normalised by inlet velocity ($v^* = v_x / v_{in}$) and height of the chamber ($Z^* = z/H$), respectively. The figure shows a rather similar trend for the x-velocity magnitude in different cases. It can be observed that values of the velocity increase significantly between Z^*=0.8 and Z^*=0.9, which are due to the airflow discharged from the inlet vent. Comparison of graphs shows a good agreement between the numerical results and experimental data. In order to evaluate quantitatively the deviation of numerical results from the experimental data, the root-mean-square-deviation (RMSD) was evaluated for different values of velocity inlet, defined as:

$$RMSD = \sqrt{\frac{\sum_{i=1}^{N} \left([\varphi_{Exp}]_i - [\varphi_{Num}]_i \right)^2}{N}} \tag{17}$$

The RMSD of simulated velocity magnitude from the measured data for v_{in} =0.111, 0.278 and 0.444 is equal to 0.032, 0.053 and 0.079, respectively.

4. Results and discussion

4.1. Assessment of different ventilation scenarios

Contours of the air velocity magnitude on the mid-section plane (Fig. 1) for different ventilation strategies are illustrated in Fig. 4. The results are presented for the intermediate inlet velocity, namely 0.1 m/s, corresponding to 0.4 ACH. For the up-supply ventilation cases, i.e. *S*-1, *S*-2 and *S*-5, the figure shows that the fresh air enters the room and flows under forced convection before ascending along the side wall towards the floor due to its lower density. Then, this air stream is merged with the buoyant upward flow created by the heat flux at floor surface. For down-supply cases, on the other hand, the discharged air from the inlet vent traverses a shorter path before approaching the floor and joining the upward buoyant airflow.

Comparisons between different scenarios indicate that the distribution of velocity magnitude on the mid-plane varies remarkably in each

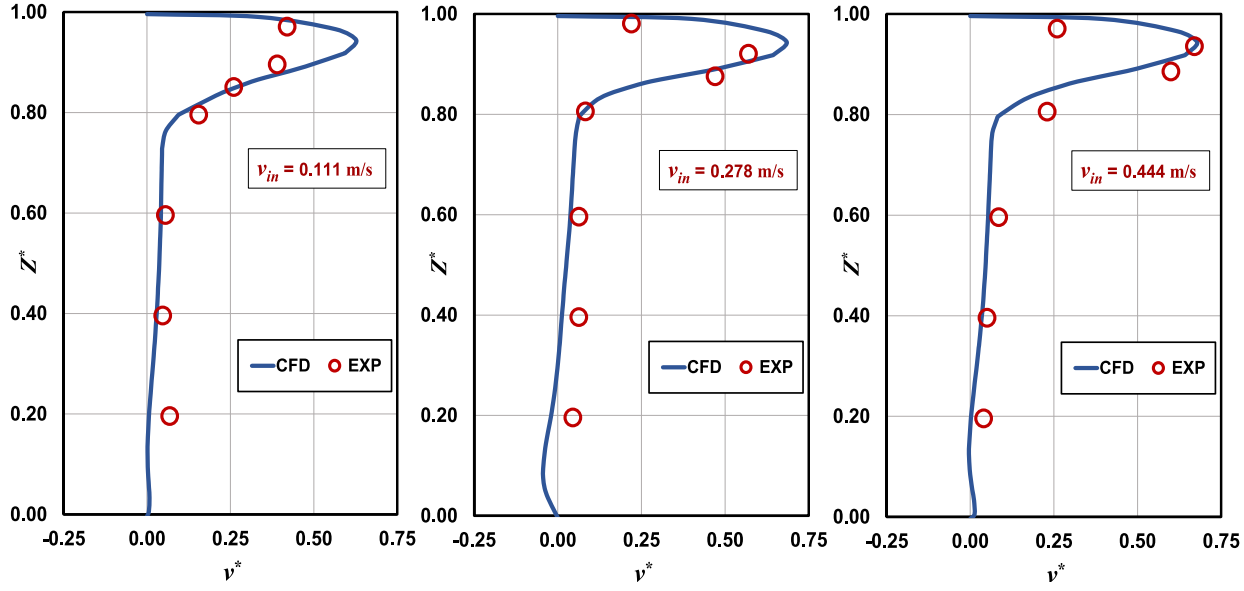

Fig. 3. Comparison of normalised *x*-velocity along mid-line of the test chamber for three inlet velocities; 0.111, 0.278 and 0.444 m/s: Experiments vs. simulations.

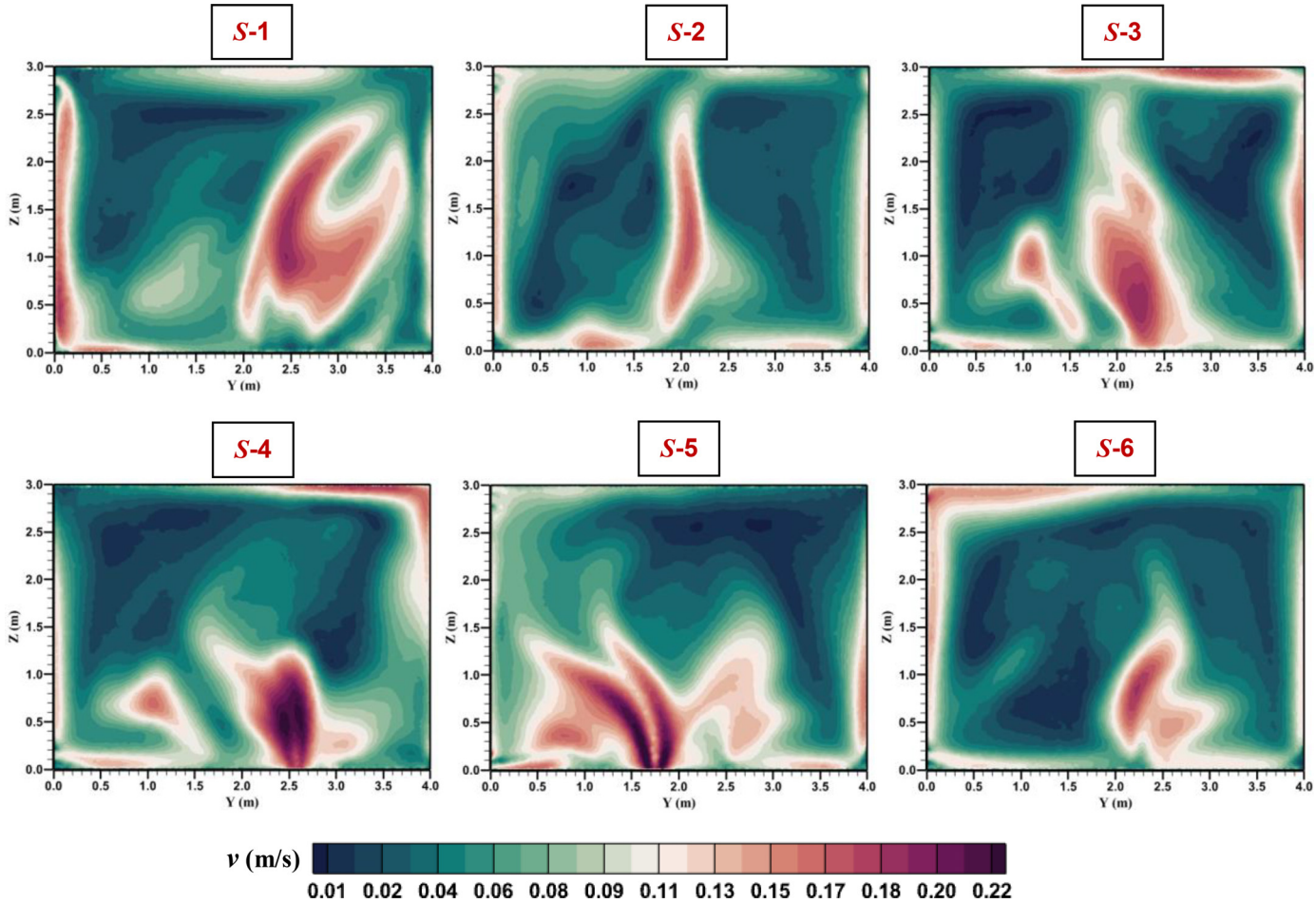

Fig. 4. Contours of the air velocity magnitude on the mid-section plane for various ventilation scenarios.

ventilation strategy. Nonetheless, it can be observed that the highest air velocity magnitude in all cases belongs to the plume formed in mid-part of the room due to the buoyancy force. amongst different cases, the highest air velocity in the plume belongs to *S*-4 and *S*-5 where it reaches to 0.22 m/s. In addition, the room mean air velocity for all cases is rather similar, ranging from 0.064 to 0.071 m/s.

Similarly, Fig. 5 compares the air temperature distribution over the mid-section plane for various scenarios. The figure shows that heat flux emitted from the floor surface disarranges the stratification of the temperature on the mid-section plane. Contours imply that the configuration of ventilation vents can affect significantly the temperature distribution and, particularly, the formation of plumes in the lower half of the room.

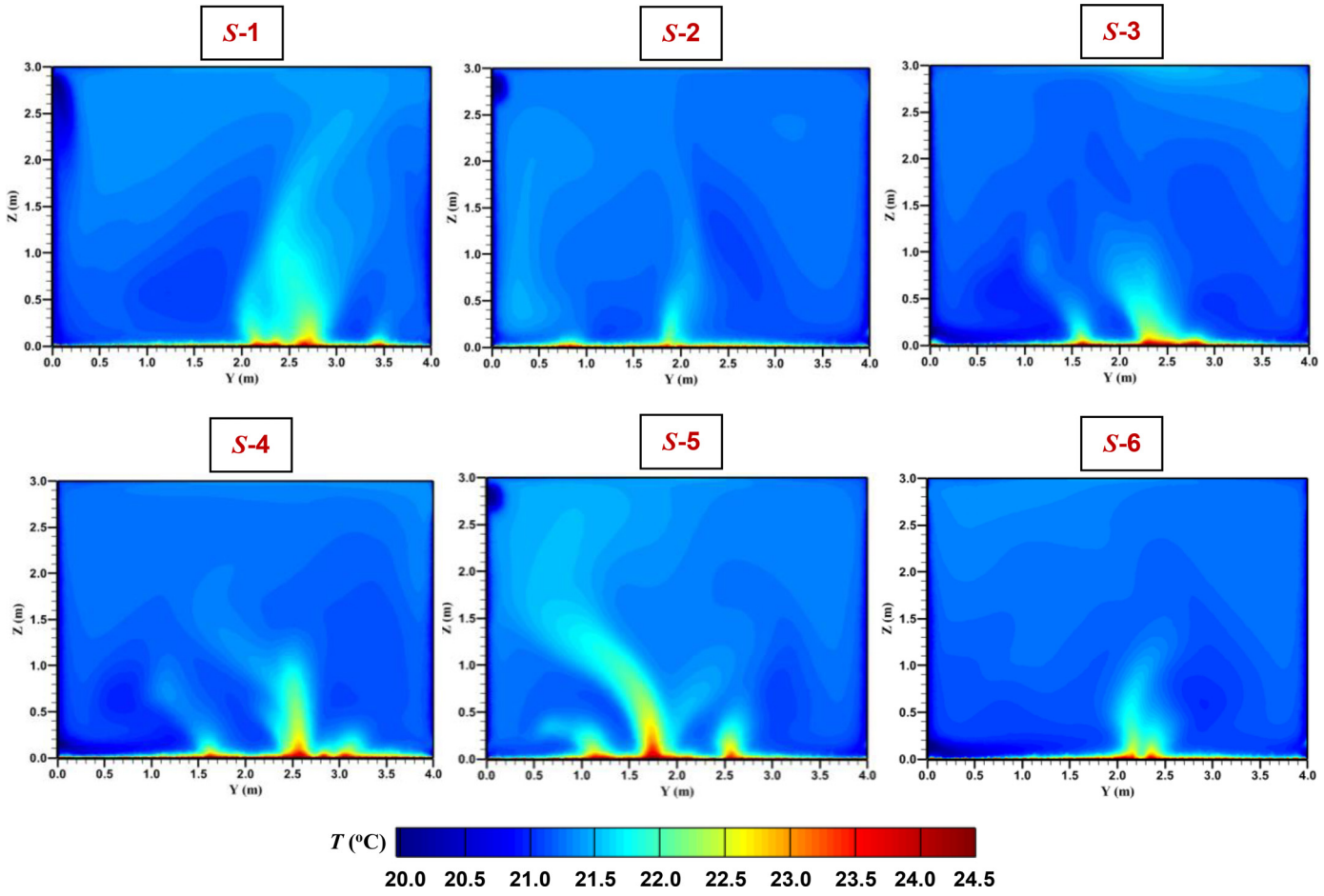

Fig. 5. Distribution of the air temperature on the mid-section plane for different ventilation scenarios.

It is evident from the figure that the highest air temperature in all cases belongs to the air flow in vicinity of the floor surface (24.5 °C) and that the airflow in vicinity of the inlet vent has the lowest air temperature (20 °C). The room mean air temperature differs slightly in each case which can be considered equal to 21.30 °C (± 0.15 °C).

For various ventilation strategies, Fig. 6 compares the normalised age of the air (τ^*) on horizontal mid-plane in breathing zone at 0.4 ACH, marked with red line in Fig. 1. The figure shows that the local age of the air is distributed non-uniformly on the horizontal plane. It demonstrates that, for up-supply cases, namely *S*-1, *S*-2 and *S*-5, the local age of the air in vicinity of the wall with inlet vents (near X axis) is lower to some extent than that in vicinity of the opposite wall containing the outlet vents.

On the other hand, the distribution trend for down-supply scenarios, particularly *S*-3 and *S*-4, is in reverse direction to up-supply cases. The reason can be explained by contours of Figs. 4 and 5, where the supply airflows in *S*-1 and *S*-2 cases counteract the buoyant airflow caused by the floor heating system on the left half of the room. Therefore, it facilitates the delivery of fresh air into the breathing zone. A comparison between different scenarios shows that the normalised age of the air on the horizontal mid-plane of breathing zone is by far lower in up-supply ventilation cases (often $\tau^*<0.97$) compared to that in down-supply strategies.

In order to compare quantitatively the volume-averaged values of the age of the air in breathing zone, Fig. 7 compares values of Ω in different cases under three different ventilation rates, namely 0.2, 0.4 and 0.6 ACH. For a given ventilation rate, the figure shows that values of Ω in up-supply scenarios (*S*-1, *S*-2 and *S*-5) are always larger than zero, indicating a lower mean age of the air in the breathing zone than the nominal age of the air. On the contrary, age of the air in the breathing zone of down-supply ventilation strategies takes negative values, except *S*-4 at highest ventilation rate. For down-supply ventilations, it can be observed that, utilising the down vent for exhaust air (*S*-4), instead of the up vent (*S*-3), can improve to some extent the delivery of fresh air into the breathing zone of floor heating systems. Among different ventilation strategies, in terms of the air quality in the breathing zone, *S*-1 is the best scenario for all ventilation rates, while *S*-3 is the worst one; for 0.2 ACH, the value of Ω in *S*-1 is 189% larger than *S*-3, corresponding to more than 314 s difference. It can be also observed from the figure that increasing the ventilation rate improves the delivery of fresh air into the breathing zone in all ventilation scenarios. However, it is evident that the enhancement rate of the Ω in each ventilation scenario differs strikingly.

Indeed, the results obtained for different ventilation scenarios confirm clearly the fact that the nominal time constant, i.e. nominal age of the air, cannot be considered as a precise criterion to guarantee the minimum required air change rate in an occupied space since the nominal age of the air could differ from the local age of the air, due to the nature of indoor air movement.

Another useful parameter to be addressed is the ventilation effectiveness in breathing zone (E_{bz}), defined as the ratio of age of the air at outlet vent to the mean age of the air in the breathing zone. In fact, values of E_{bz} larger than 1.0 indicates a satisfactory effectiveness of the ventilation strategy in the breathing zone. A comparison between results of Figs. 7 and 8 implies that there is a direct qualitative relation between values of Ω and *E* in all ventilation rates: A larger value of Ω is associated with a better ventilation effectiveness (E_{bz}). Hence, for a given ACH, up-supply scenarios demonstrate a higher ventilation effec-

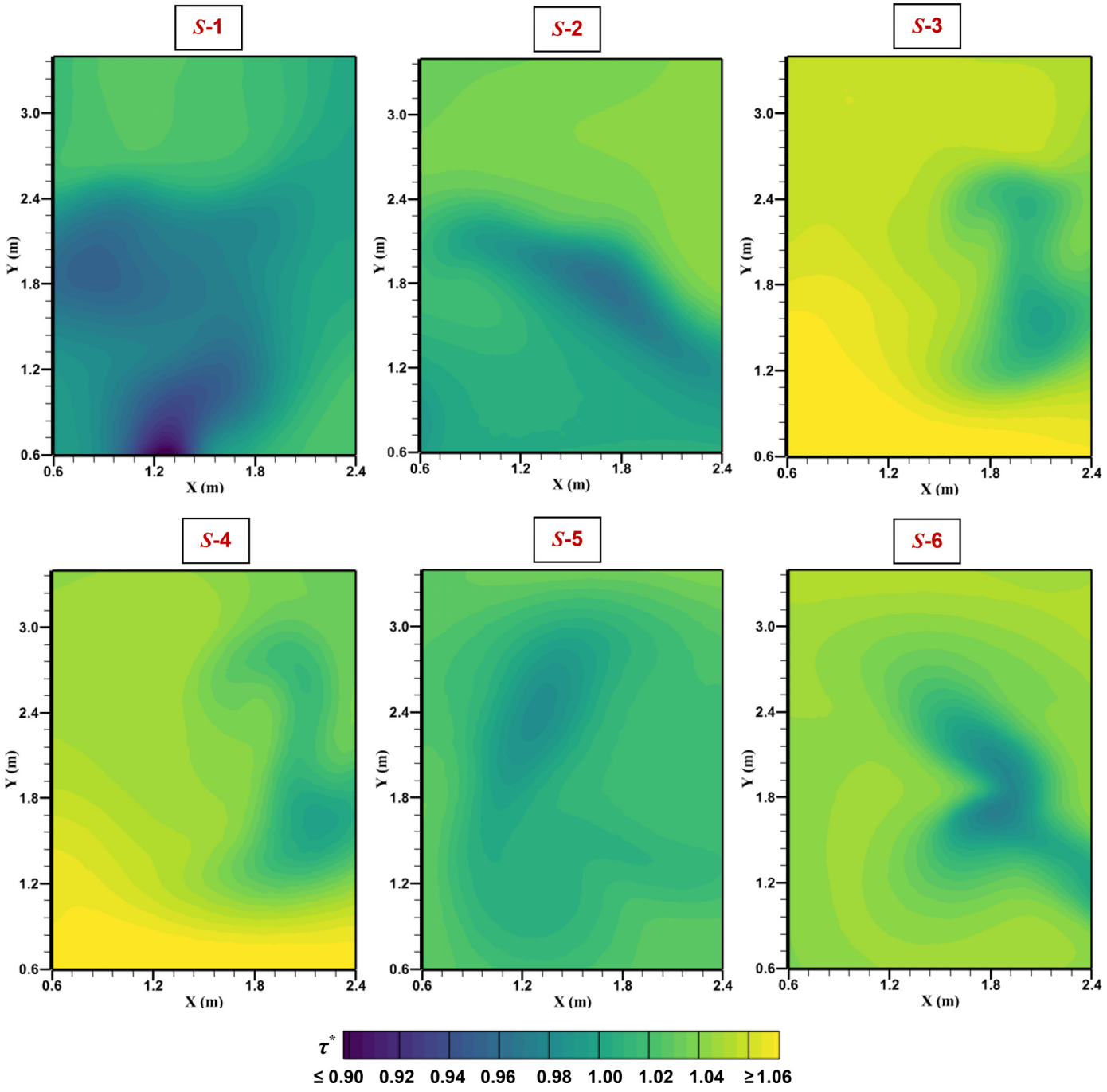

Fig. 6. Contours of the normalised age of the air on horizontal mid-plane in breathing zone for different ventilation strategies.

tiveness compared to down-supply cases. For instance, at 0.6 ACH, *S*-1 and *S*-2 render 2.7% and 1.6%, respectively, larger values of E_{bz} than *S*-3. Furthermore, as expected, the ventilation effectiveness in all scenarios improves with increase in inlet velocity of supply air. It is noteworthy to mention that evaluation of room air change efficiency (*RACE*) parameter for different cases showed the similar trend to E_{bz}, which for the sake of brevity is not presented here.

To survey main reasons of various distribution of mean age of the air in the breathing zone of each scenario, Fig. 9 depicts contours of τ^* with streamlines on mid-section plane of the room at 0.4 ACH. The breathing zone in each scenario has been marked with red dashed-lines. A comparison between different scenarios shows a significant difference in airflow pattern and age of the air distribution over the mid-section plane. Streamlines in all cases indicate a general upward airflow field due to the prominent impact of the warm floor and natural convection. Nonetheless, it can be observed that for up-supply strategies, particularly for *S*-1 and *S*-2, the airflow discharged from the inlet weakens this phenomenon in the breathing zone, at least in the half of the plane adjacent to the inlet vent. Therefore, a younger age of the air in the breathing zone of these scenarios can be seen (τ^*<0.96), compared to down-supply strategies. On the other side, for down-supply cases, namely *S*-3, *S*-4 and *S*-6, the youngest age of the air can be observed in vicinity of the floor (under breathing zone) due to the supply airflow pattern. Another issue to be mentioned is on the role of vortex flows in down-supply scenarios. It is evident from streamlines of *S*-3 and *S*-4 that large eddy currents can bring back the upper stale air (adjacent to the ceiling) into the in-

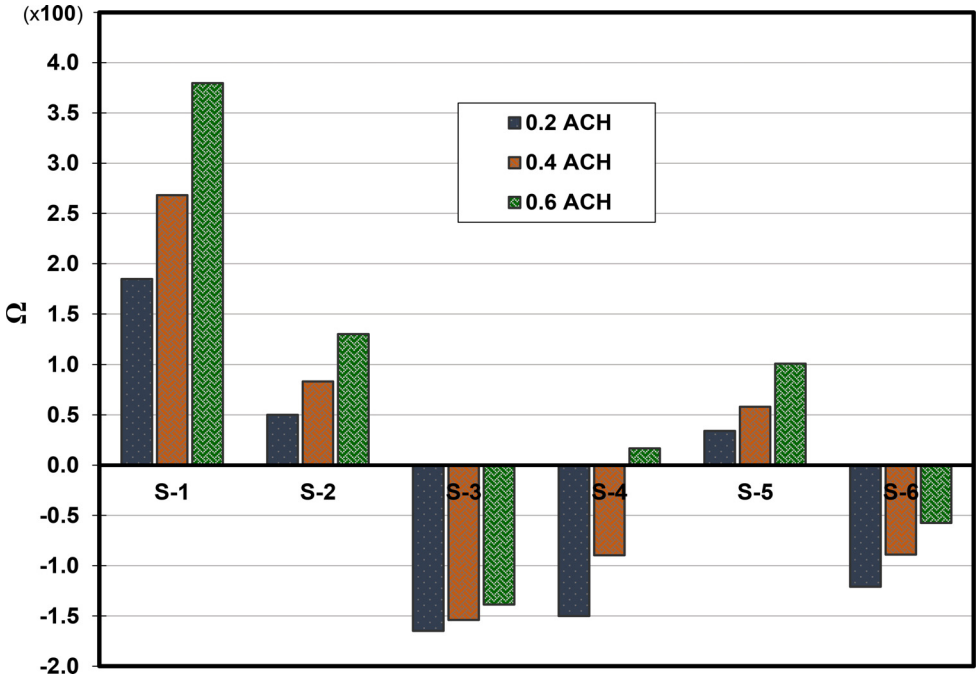

Fig. 7. Comparison between values of Ω in different ventilation scenarios for three ventilation rates, namely 0.2, 0.4 and 0.6 ACH.

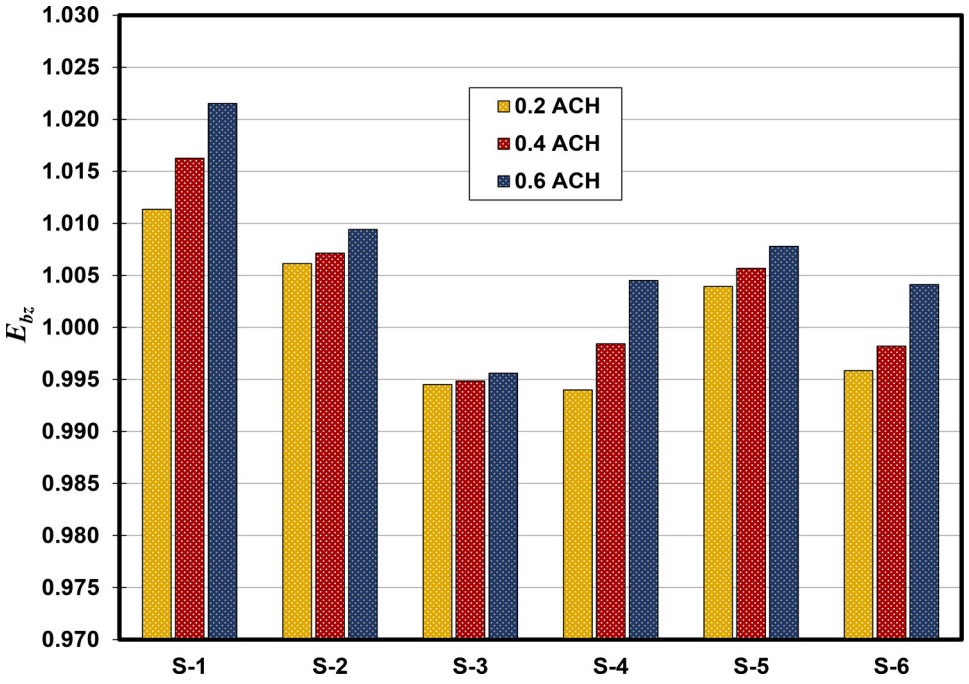

Fig. 8. Ventilation effectiveness (E_{bz}) in the breathing zone for different ventilation scenarios at three air change rates.

let air path, preventing a better delivery of fresh air to the breathing zone.

4.2. Role of the floor temperature

In the previous section, the efficiency of six different ventilation scenarios in terms of the air quality in the breathing zone was evaluated, for a given floor temperature and inlet supply temperature. In the present section, effect of the floor temperature on the fresh air distribution in the breathing zone is evaluated. In this context, two utmost up- and down-supply scenarios, namely *S*-1 and *S*-3, are considered to be compared in four different floor temperature levels and at a given ventilation rate (0.4 ACH).

Indeed, different floor temperature levels have influence on the distribution of indoor airflow. With increase of the floor temperature, the impact of the natural convection is augmented, affecting the delivery pattern of supply air into the breathing zone. In this context, the importance of natural convection relative to the forced convection can be addressed by employing theory of Richardson number (*Ri*), which can be evaluated by using a combination of the Grashof number (*Gr*) and Reynolds number (*Re*) as: $Ri=Gr/Re^2$.

Fig. 10 illustrates the role of characteristic floor temperature θ_f in variations of Ω and the *Ri* for two ventilation scenarios. The figure shows that by increasing θ_f, the role of natural convection becomes more prominent and the *Ri* therefore increases linearly with θ_f. Meanwhile, the figure indicates that an increase in the *Ri* leads to a reverse trend

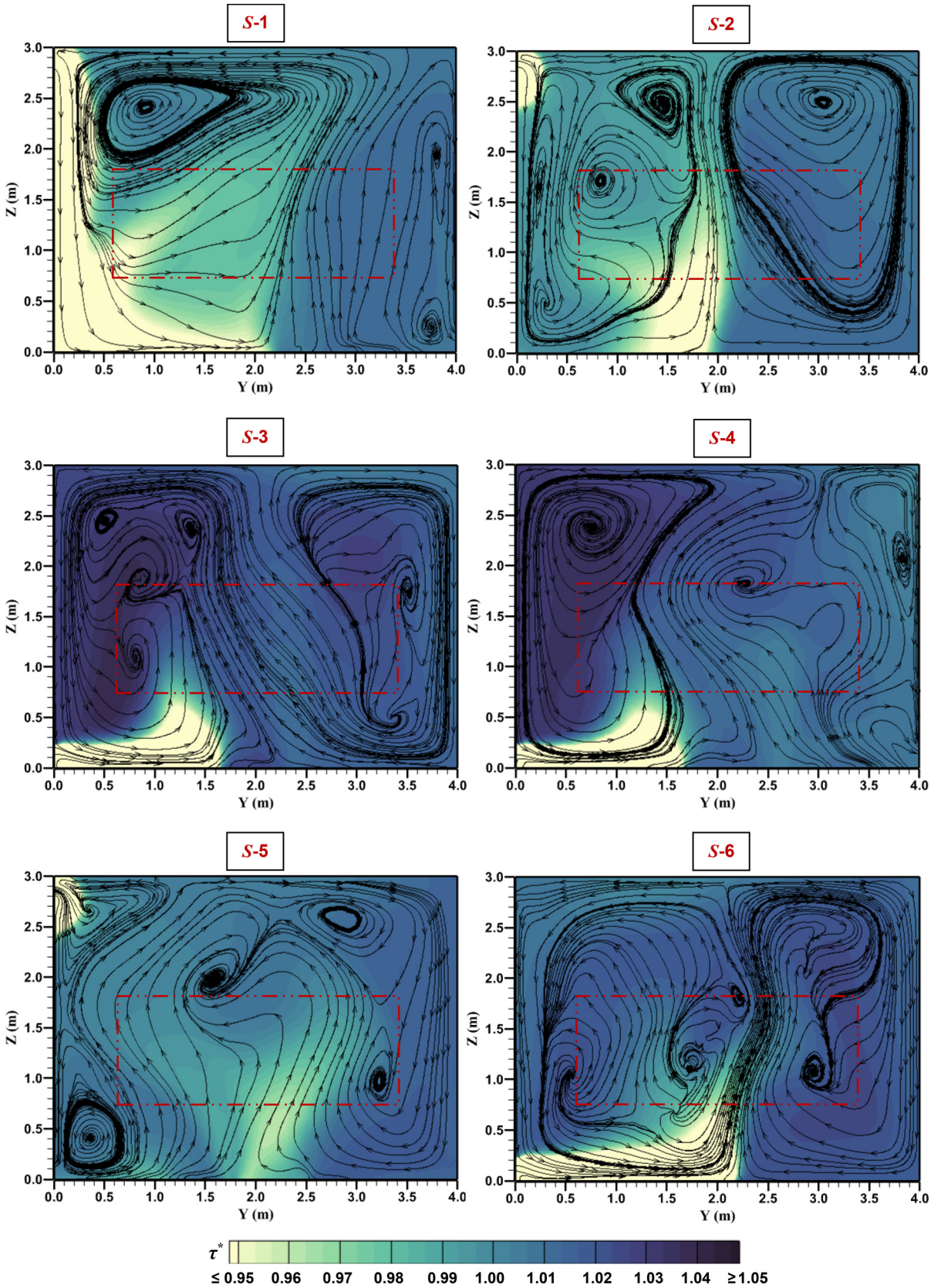

Fig. 9. Streamlines and contours of normalised age of the air on mid-section plane in different cases.

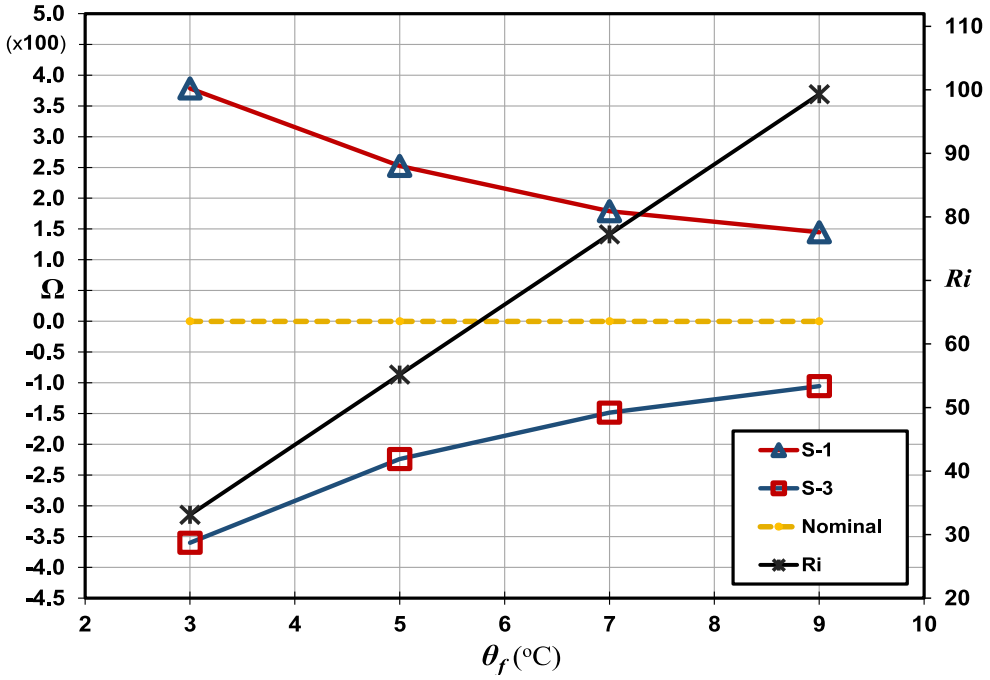

Fig. 10. Variations in Ω triggered by changes in the characteristic floor temperature (θ_f) for *S*-1 and *S*-3: Effect of the Richardson number (*Ri*).

Table 5
A comparison between various parameters in up- and down-supply ventilation scenarios at different floor temperature levels.

Scenario	θ_f (˚C)	Q_f (W)	T (˚C)	τ^*	E_{bz}	*RACE* [%]
S-1	3	235.1	20.75	0.978	1.028	51.08
S-1	5	451.2	21.34	0.983	1.015	50.75
S-1	7	585.6	21.77	0.991	1.010	50.48
S-1	9	759.2	22.45	0.993	1.008	50.31
S-3	3	231.9	20.77	1.017	0.981	49.38
S-3	5	442.2	21.36	1.013	0.992	49.61
S-3	7	576.0	21.79	1.008	0.995	49.72
S-3	9	754.2	22.38	1.005	0.998	49.80

in the variation of Ω in each ventilation scenarios; the value of Ω in up-supply mode (*S*-1) decreases with increase of the *Ri* while in down-supply mode (*S*-3) an increase in *Ri* improves the delivery of fresh air into the breathing zone. Nonetheless, its noticeable that, even at the highest considered value of θ_f, the value of Ω in up-supply scenario remains larger than nominal age of the air (+1.44) and that in the down-supply one is still negative (−1.05), implying a younger air in the breathing zone of *S*-1.

Table 5 reports values of the required thermal energy (Q_f), volume-averaged air temperature (T), normalised age of the air in the breathing zone (τ^*), ventilation effectiveness in the breathing zone (E_{bz}), and room air change efficiency (*RACE*) for two ventilation strategies at different floor temperature levels. A comparison between values of τ^* and E_{bz} for different values of θ_f confirms that the delivery of fresh air in up-supply mode (*S*-1) is more efficient compared to down-supply one (*S*-3). In addition, regarding the room air change efficiency (*RACE*), it can be observed that, unlike *S*-1 scenario, values of *RACE* in *S*-3 are less than 50% for any value of θ_f, indicating the insufficient level of room ventilation in this scenario at the given ACH (0.4).

In terms of the required thermal energy, it can be observed that, by employing *S*-1 scenario at lower values of θ_f, a better indoor air quality with a significant lower energy consumption can be achieved compared to *S*-3 scenario. However, this better air quality and energy saving is at penalty of a slight decrease in the mean air temperature inside the room.

4.3. Impact of the supply air temperature

Effect of the inlet supply air temperature on the age of the air and ventilation effectiveness in the breathing zone are investigated in the present section. Fig. 11 shows variations of Ω and E_{bz} with characteristic inlet temperature difference (θ_{in}) for two ventilation scenarios, namely *S*-1 and *S*-3, at a given ventilation rate (0.4 ACH) and floor temperature (25 ˚C).

The figure shows that values of Ω and E_{bz} in *S*-1 are significantly larger than those in *S*-3, except when θ_{in}>0. While increase of the inlet supply temperature improves Ω in down-supply scenario, it weakens delivery of the fresh air in breathing zone of up-supply scenario. For instance, an increase in θ_{in} from −4.0 ˚C to −2.0 ˚C results in an 8.2% reduction of Ω in *S*-1, whereas the same increase in θ_{in} leads to an 8.7% increment of Ω in *S*-3. The same trend can be also observed for E_{bz}. It is evident from the figure that, as the value of θ_{in} increases, plots of Ω in each scenario converge almost symmetrically to the nominal age of the air (Ω =0). However, it is noticeable that when θ_{in}>0, the rate of changes in Ω increases drastically in both ventilation scenarios.

In fact, the results of Fig. 11 can be explained by the role of buoyancy force inside the room; a higher inlet temperature amplifies the upward buoyant airflow driven by the floor heating system. In down-supply scenario, this issue can facilitate the delivery of fresh air into the breathing zone. On the contrary, in up-supply ventilation mode, this augmented upward airflow would prolong the delivery of fresh air delivery to the breathing zone. In both ventilation modes, when the inlet air temperature is higher than the temperature of side wall adjacent to the inlet vent, i.e. θ_{in}>0, this effect becomes more striking, namely the larger rate of changes in Ω. Nonetheless, it should be noted that the discussion here revolves around the spaces with a rather low air change rate.

5. Verification of obtained results

In order to verify the obtained numerical results, the decay rate of CO_2 in the breathing zone of up- and down-supply cases, namely *S*-1 and *S*-3, is compared for two values of the characteristic floor temperature, namely θ_f =3 and 5 ˚C. In this context, the CO_2 representing the indoor contaminant was firstly distributed uniformly inside the domain with concentration of 1.8 g/m^3 equal to 1000 ppm. Then, transient simula-

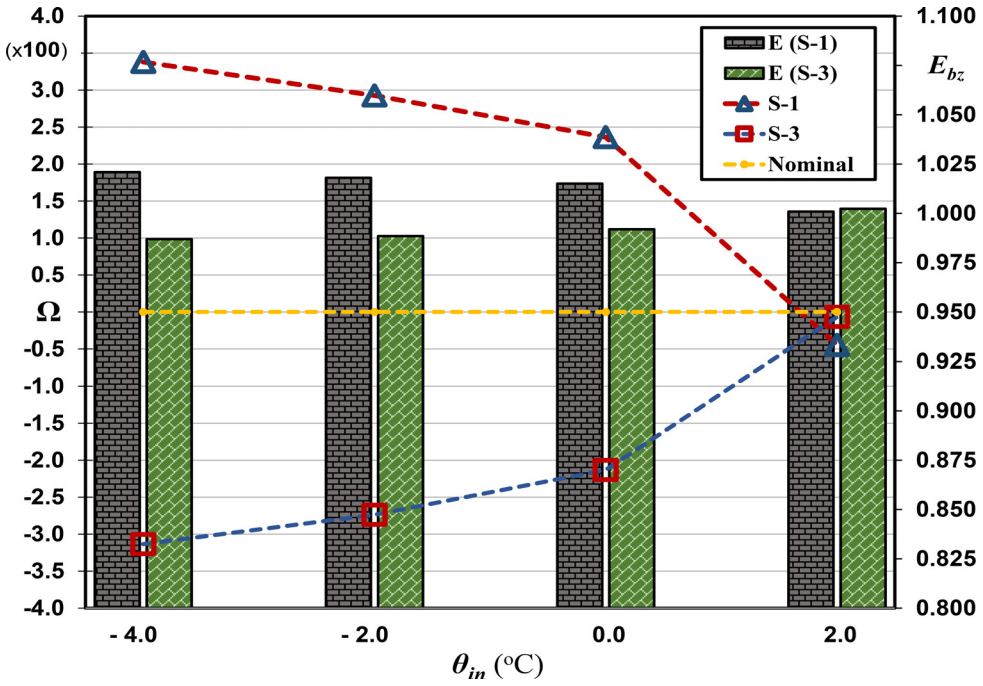

Fig. 11. Variation of Ω and E_{bz} with the supply inlet temperature in two ventilation scenarios: *S*-1 and *S*-3.

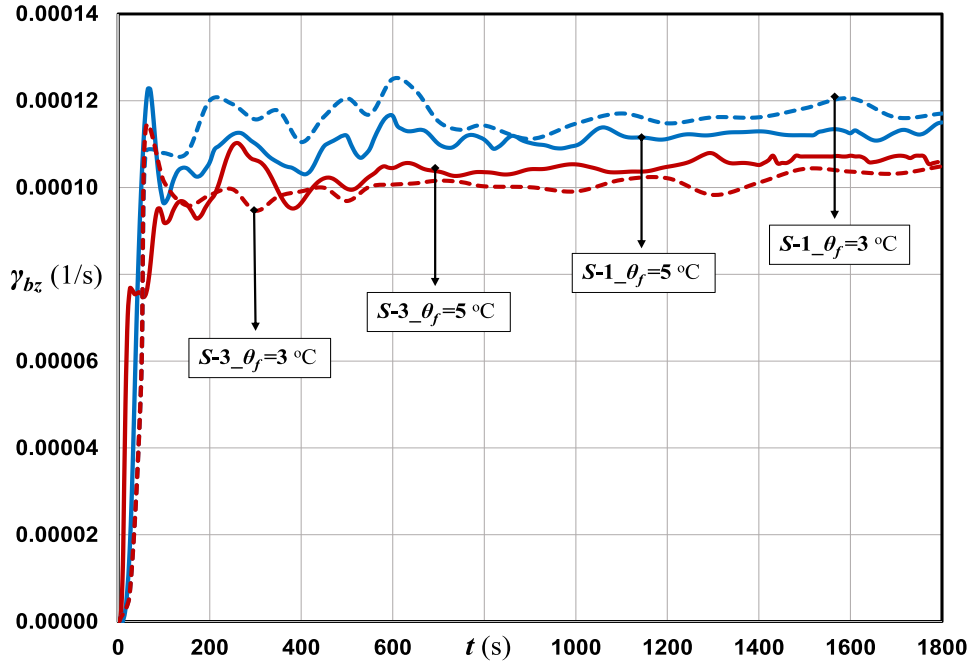

Fig. 12. Time evolution of the CO_2 decay rate in the breathing zone (γ_{bz}) of four considered cases: *S*-1 and *S*-3 with θ_f =3 and 5 °C.

tions was performed to monitor the decay rate of the CO_2 in the breathing zone of each case. The numerical setup is identical to that presented in Section 2, except solving a time-dependant species transport model to determine the concentration of CO_2. The decay rate of the contaminant in the breathing zone can be given as [33,34]:

$$\gamma_{bz} = -\ln(C(t)/C(0))/t \quad (18)$$

where $C(t)$ and $C(0)$ represent the concentration of CO_2 in the breathing zone at times t and 0, respectively.

Fig. 12 compares the time evolution of $\gamma_{bz}$for considered cases during 1800s, at a given ventilation flow rate (0.4 ACH). The figure shows that *S*-1 renders a higher decay rate compared to *S*-3, and that increasing the floor temperature leads to a reverse trend in variation of the CO_2 removal in the breathing zone of up- and down-supply scenarios; regardless of a very first minutes, the results indicate that a 2 °C decrease in the floor temperature of *S*-1 results in mean 3.8% augmentation of γ_{bz}, while the same decrease in the floor temperature of *S*-3 leads to mean 2.3% decrease of γ_{bz}. A comparison between graphs confirms the results presented in Figs. 7 and 10.

6. Conclusions

In the present study, the distribution of local age of the air in the breathing zone of floor heating systems under various ventilation scenarios was investigated. A computational fluid dynamic (CFD) model was established, validated against experimental data, to evaluate the turbulent airflow field, temperature distribution and local mean age of

the air as well as to obtain relevant indicators for indoor air quality (IAQ). Six different ventilation scenarios at three ventilation rates were regarded in order to find the optimal ventilation design in terms of the better delivery of the fresh air. Furthermore, the integrated effects of the floor temperature and inlet supply temperature along with the ventilation design on the distribution of local age of the air were addressed. Finally, the obtained results were verified by monitoring the CO_2 decay rate in the breathing zone of various cases. The results obtained for different ventilation scenarios implied that the nominal age of the air cannot be considered as a precise criterion to guarantee the minimum required air change rate in an occupied space since the nominal age of the air could differ from the local age of the air due to the nature of indoor air movement.

The main findings of the present study based on the obtained results can be concluded as follows:

- A comparison between considered ventilation scenarios indicated that the up-supply ventilation mode is more efficient than down-supply one in terms of the ventilation effectiveness and delivery of fresh air in the breathing zone. To be more precise, for a given floor temperature and supply air condition, up-supply and down-exhaust configuration (*S*-1) rendered the youngest age of the air in the breathing zone while the down-supply and up-exhaust configuration (*S*-3) was the worst scenario.
- For a given floor and supply air temperature, increasing the ventilation rate enhanced the delivery of fresh air into the breathing zone for all ventilation scenarios. However, it was shown that the improvement rate of age of the air with ventilation rate varies significantly in each strategy.
- It was revealed that alterations in the floor temperature leads to a reverse trend in the variation of mean age of the air in up- and down-supply scenarios; for up-supply mode (*S*-1), mean age of the air in the breathing zone increased with increment of the *Ri* (Richardson number), while an increase in *Ri* improved the delivery of fresh air in down-supply mode (*S*-3).
- For a given floor temperature, reducing the characteristic inlet temperature, θ_{in}, namely the temperature difference between inlet supply and surrounding walls, improved delivery of the fresh air in breathing zone of up-supply scenario. On the other hand, for down-supply ventilation, increase of the inlet supply temperature, i.e. a larger value of θ_{in}, resulted in a younger age of the air in the breathing zone.

Declaration of competing interest

The authors declare that they have no known competing financial interests or personal relationships that could have appeared to influence the work reported in this paper.

The authors declare the following financial interests/personal relationships which may be considered as potential competing interests:

CRediT authorship contribution statement

Aminhossein Jahanbin: Conceptualization, Methodology, Software, Validation, Data curation, Investigation, Writing – original draft. **Giovanni Semprini:** Supervision, Conceptualization, Visualization, Writing – review & editing.

References

[1] S. Torresin, G. Pernigotto, F. Cappelletti, A. Gasparella, Combined effects of environmental factors on human perception and objective performance: a review of experimental laboratory works, Indoor Air 28 (4) (2018) 525–538.

[2] E.Z. Świercz, Improvement of indoor air quality by way of using decentralised ventilation, J. Building Eng. 32 (2020) 101663.

[3] C. Ren, C. Xi, J. Wang, Z. Feng, F. Nasiri, S.-J. Cao, F. Haghighat, Mitigating COVID-19 infection disease transmission in indoor environment using physical barriers, Sustainable Cities and Society 74 (2021) 103175.

[4] I. Annesi-Maesano, M. Hulin, F. Lavaud, C. Raherison, C. Kopferschmitt, F. de Blay, D. André Charpin, C. Denis, Poor air quality in classrooms related to asthma and rhinitis in primary schoolchildren of the French 6 cities study, Thorax 67 (2012) 682–688.

[5] H.S. Chu, H.C. Yu, W. Mui, L.T. Wong, Ventilation of general hospital wards for mitigating infection risks of three kinds of viruses including Middle East respiratory syndrome Coronavirus, Indoor and Built. Environ. 26 (4) (2016) 514–527.

[6] A. Murga, Z. Long, S.-J. Yoo, E. Sumiyoshi, K. Ito, Decreasing inhaled contaminant dose of a factory worker through a hybrid emergency ventilation system: performance evaluation in worst-case scenario, Energy and Built Environ. 1 (3) (2020) 319–326.

[7] T. Arghand, T. Karimipanah, H.B. Awbi, M. Cehlin, U. Larsson, E. Linden, An experimental investigation of the flow and comfort parameters for under-floor, confluent jets and mixing ventilation systems in an open-plan office, Building and Environ. 92 (2015) 48–60.

[8] L. Koufi, Y. Younsi, Y. Cherif, H. Naji, Numerical investigation of turbulent mixed convection in an open cavity: effect of inlet and outlet openings, Int. J. Thermal Sci. 116 (2017) 103–117.

[9] A. Bouras, S. Bouabdallah, B. Ghernaout, M. Arıcı, Y. Cherif, E. Sassine, 3D numerical simulation of turbulent mixed convection in a cubical cavity containing a hot block, J. Appl. Fluid Mechan. 14 (6) (2021) 1869–1880.

[10] D. Chati, S. Bouabdallah, B. Ghernaout, E. Tunçbilek, M. Arıcı, Z. Driss, Turbulent mixed convective heat transfer in a ventilated enclosure with a cylindrical/cubical heat source: a 3D analysis, Energy Sources, Part A: Recovery, Utilization, and Environ. Effects (2021) 1–18, doi:10.1080/15567036.2021.1923872.

[11] R. Zhuang, X. Li, J. Tu, CFD study of the effects of furniture layout on indoor air quality under typical office ventilation schemes, Building Simulation 7 (7) (2014) 263–275.

[12] A. Jahanbin, Efficacy of coupling heat recovery ventilation and fan coil system in improving the indoor air quality and thermal comfort condition, Energy and Built Environ. 3 (4) (2022) 478–495.

[13] A. Meiss, J. Feijó-Muñoz, M. García-Fuentes, Age-of-the-air in rooms according to the environmental condition of temperature: a case study, Energy & Buildings 67 (67) (2013) 88–96.

[14] ISO16000-8Determination of Local Mean Ages of Air in Buildings for Characterizing Ventilation Conditions, Geneva, 2007.

[15] M. Ning, S. Mengjie, C. Mingyin, P. Dongmei, D. Shiming, Computational fluid dynamics (CFD) modelling of air flow field, mean age of air and CO2 distributions inside a bedroom with different heightsof conditioned air supply outlet, Appl. Energy 164 (2016) 906–915.

[16] C. Buratti, R. Mariani, E. Moretti, Mean age of air in a naturally ventilated office: experimental data and simulations, Energy & Buildings 43 (2011) 43 2021–2027.

[17] S.F. Diaz-Calderon, J.A. Castillo, G. Huelsz, Indoor air quality evaluation in naturally cross-ventilated buildings for education using age of air, J. Phys.: Conference Series (2021) 2069 012182.

[18] H. Ahn, D. Rim, L.J. Lo, Ventilation and energy performance of partitioned indoor spaces under mixing and displacement ventilation, Building Simulation (11) (2018) 561–574.

[19] G. Gan, Effective depth of fresh air distribution in rooms with single-sided natural ventilation, Energy & Buildings 31 (2000) 65–73.

[20] C.F. Gao, W.L. Lee, Evaluating the influence of openings configuration on natural ventilation performance of residential units in Hong Kong, Building and Environ. 46 (2011) 961–969.

[21] S.-J. Cao, H.-Y. Deng, Z. Zhou, Y. Deng, Ventilation inlets design based on ventilation performance assessment using a dimensionless time scale, Indoor and Built Environ. 28 (8) (2019) 1049–1063.

[22] T. Chen, Z. Feng, S.-J. Cao, The effect of vent inlet aspect ratio and its location on ventilation efficiency, Indoor and Built Environ. 29 (2) (2020) 180–195.

[23] ASHRAE*Ventilation For Acceptable Indoor Air Quality;* ASHRAE Standard 62.1 - *2016*, ASHRAE, Atlanta, GA, USA, 2016.

[24] Y. Zhou, Y. Deng, P. Wu, S.-J. Cao, The effects of ventilation and floor heating systems on the dispersion and deposition of fine particles in an enclosed environmen, Building and Environ. 125 (2017) 192–205.

[25] ASHRAE, ANSI/ASHRAE STANDARD 55Thermal Environmental Conditions For Human Occupancy, Atlanta, USA, 2017.

[26] T. Chen, S.-J. Cao, Numerical study on the integrated effects of supplied air velocity and exhaust velocity on particles removal for industrial buildings, Energy and Built Environment 2 (4) (2021) 390–391.

[27] A. Jahanbin, G. Semprini, Combined impacts of the ceiling radiant cooling and ventilation on dispersion and deposition of indoor airborne particles, Thermal Sci. Eng. Progress 34 (2022) 101438.

[28] Q. Chen, Comparison of different k-e models for indoor airflow computations, Numerical Heat Transfer, Part B: Fundementals 28 (1999) 4391–4409.

[29] H. Versteeg, W. Malalasekera, An Introduction to Computational Fluid dynamics: the Finite Volume Method, 2nd ed., Pearson - Prentice Hall, 2007.

[30] A. Jahanbin, G. Semprini, Numerical study on indoor environmental quality in a room equipped with a combined HRV and radiator system, Sustainability 12 (24) (2020) 10576.

[31] V. Chanteloup, P. Mirade, Computational fluid dynamics (CFD) modelling of local mean age of air distribution in forced-ventilation food plants, J. Food Eng. 90 (2009) 90–103.

[32] D. Etheridge, M. Sandberg, Building Ventilation Theory Measurements, John Wiley & Sons, Baffins Lane, 1996.

[33] A. Jahanbin, G. Semprini, Integrated effects of the heat recovery ventilation and heat source on decay rate of indoor airborne particles: a comparative study, J. Building Eng. 50 (2022) 104156.

[34] X. Chen, A. Li, An experimental study on particle deposition above near-wall heat source, Build. Environ. 81 (2014) 131–149.